Available online at www.sciencedirect.com
SCIENCE DIRECT®
International Journal of Heat and Mass Transfer 47 (2004) 3327–3340
International Journal of HEAT and MASS TRANSFER
www.elsevier.com/locate/ijhmt

Transient heating of diesel fuel droplets

S.S. Sazhin [a,*], P.A. Krutitskii [b], W.A. Abdelghaffar [a], E.M. Sazhina [a], S.V. Mikhalovsky [c], S.T. Meikle [c], M.R. Heikal [a]

[a] School of Engineering, Faculty of Science and Engineering, University of Brighton, Cockcroft Building, Lewes Road, Brighton BN2 4GJ, UK
[b] Faculty of Physics, Moscow State University, Vorobyovy gory, Moscow 119899, Russia
[c] School of Pharmacy and Biomolecular Sciences, University of Brighton, Cockcroft Building, Brighton BN2 4GJ, UK

Received 24 February 2003; received in revised form 24 January 2004
Available online 19 March 2004

Abstract

New solutions of the heat conduction equation inside a spherical droplet are obtained. The droplet is assumed to be heated by convection and radiation from the surrounding hot gas—a situation typical in many engineering applications. Initial droplet evaporation and the effects of time dependent gas temperature and convection heat transfer coefficient are taken into account. In the cases of constant, and almost constant convection heat transfer coefficients, the explicit formulae for time dependent radial distribution of temperature inside droplets are obtained. In the case of arbitrary convection heat transfer coefficient, the differential equations are reduced to the Volterra integral equation of the second kind. A numerical scheme for the solution of this equation is suggested. The solution for constant convection heat transfer coefficient is applied to a typical problem of fuel droplet heating in a diesel engine. It is shown that finite thermal conductivity of fuel droplets and the effects of radiation need to be taken into account when modelling droplet heating in diesel engines.

Keywords: Droplet heating; Conduction; Radiation; Diesel fuel

1. Introduction

The heating of droplets is driven by convective and radiative heat transfer from the surrounding medium. In the case of convective heating, there is an initial increase of temperature at the surface of the droplets, from where the heat is transferred to their main body. In the case of radiative heating of realistic semi-transparent droplets, the thermal radiation is absorbed inside the droplets [1,2]. Sirignano [3] considered the following classification of models for heat transfer inside droplets in order of increasing complexity: (1) constant droplet-temperature; (2) infinite liquid thermal conductivity; (3) conduction-limit; (4) effective conductivity; (5) vortex model of droplet heating; (6) Navier–Stokes solution.

Model 2 is perhaps most widely used in multidimensional commercial Computational Fluid Dynamics (CFD) codes [4–7] and analytical studies [8–10]. The main attractive feature of this model is its simplicity. However, model 3 can give a noticeable improvement in the prediction of diesel spray evaporation processes when compared with model 2 [11]. The authors of [11] suggested that a numerical solution of the heat conduction equation inside droplets is added to the solution of gas dynamics, heat transfer and chemical equations for gas phase. The addition of these calculations would certainly increase the CPU intensity of the code. It is known that model 3 may not lead to an improvement in the accuracy of computations in the case when the contribution of recirculation inside droplets is significant [3,12,13]. In this case, models 4–6 would have to be

* Corresponding author. Tel.: +44-1273-642-677; fax: +44-1273-642-301.
E-mail address: s.sazhin@brighton.ac.uk (S.S. Sazhin).

0017-9310/$ - see front matter © 2004 Elsevier Ltd. All rights reserved.
doi:10.1016/j.ijheatmasstransfer.2004.01.011

Nomenclature

a	coefficient introduced in Eq. (7)
a_λ	liquid fuel absorption coefficient
A	coefficient introduced in Appendix A
b	coefficient introduced in Eq. (7)
B	coefficient introduced in Appendix A
B_λ	Planck function
B_M	Spalding number
c	specific heat capacity
c_0	constant introduced in Eq. (B.2)
c_n	coefficients introduced in Eq. (A.1)
$C_{1,2}$	coefficients in the Planck function
$f(r)$	parameter introduced in formula (A.7)
f_n	coefficients introduced in formula (A.7)
$\|F\|$	norm of the function F
$G(t,r)$	kernel defined by formula (24)
$\widetilde{G}(t)$	function defined by formula (B.2)
h	convection heat transfer coefficient
h_0	$\frac{hR_d}{k_l}-1$
h_1	parameter introduced in formula (20)
$H(t)$	$\frac{h(t)R_d}{k_l}-1$
$I(\bar{t})$	auxiliary integral introduced in Appendix C
k	thermal conductivity
L	specific heat of evaporation
M	molar mass
$M(t)$	$h(t)T_{eff}(t)R_d/k_l$
n	index of refraction
N	number of timesteps
Nu	Nusselt number
q_n	coefficients introduced in formula (A.6)
Q_a	efficiency factor of absorption
p_n	coefficients introduced in formula (A.5)
$P(r)$	$P_1(r)/(c_l\rho_l)$
$P_1(R)$	power generated in unit volume
$\widetilde{P}$	$rP(r)$
Pe	Peclet number
Pr	Prandtl number
r	normalised radius (R/R_d)
R	radius
Re	Reynolds number
t	time
T	temperature
$\widetilde{T}_0(r)$	parameter introduced in formula (A.6)
u	Tr
$U(r,t)$	function introduced in formula (22)
$v_n(r)$	the full set of non-trivial solutions of Eq. (A.2)
$\|v_n(r)\|$	parameter introduced in Eq. (A.4)
w	normalized absorbed spectral power of radiation per unit volume
W	function introduced in Eq. (11)
Y	relative concentration

Greek symbols

$\bar{\gamma}$	parameter introduced in Eq. (E.1)
δ	small parameter introduced in Eq. (B.1)
δ_{nm}	0 if $n \neq m$, 1 if $n = m$
Δt	timestep
ϵ	small parameter introduced in formula (29)
$\eta(t)$	$h_1(t)/\epsilon$
κ	$k_l/(c_l\rho_l R_d^2)$
κ_λ	index of absorption
λ	wavelength or parameter introduced in Eq. (A.2)
λ_n	eigenvalues of Eq. (A.2)
$\mu_0(t)$	$\frac{hT_{eff}(t)R_d}{k_l}$
μ_c	parameter introduced in Eq. (E.1)
$\mu_{g0}(t)$	$-h_1(t)u+\mu_0(t)$
μ_*	parameter introduced in Eq. (E.1)
$\nu_{0,1,2,\ldots,n}$	function introduced in formula (29)
ξ	parameter introduced in formula (E.2)
ρ	density
τ	optical thickness or the argument in the integrands
τ_0	$a_\lambda R_d$
χ	k_{eff}/k_l
$\psi(t)$	function introduced in formula (C.1)

Subscripts

a	air
b	boiling
d	droplet
eff	effective
ext	external
f	fuel
fs	saturated fuel vapour
g	gas
p	constant pressure
s	surface
up	upper

applied. Direct application of models 5 and 6, however, would require considerable computational resources to take into account 3D effects [13]. Model 4, where the effect of convective heat transfer inside droplets is accounted for by replacing the actual thermal conductivity of liquid k_l by the so called effective thermal conductivity k_{eff}, seems to be a reasonable compromise between accuracy and computational efficiency. In this model it is

assumed that $k_{\text{eff}} = \chi k_{\text{l}}$, where the coefficient χ varies from about 1 (at droplet Peclet number $Pe_{\text{d(f)}} = Re_{\text{d(f)}}Pr_{\text{d(f)}} < 10$) to 2.72 (at $Pe_{\text{d(f)}} > 500$) and can be approximated as [3]: $\chi = 1.86 + 0.86\tanh[2.225\log_{10} \times (Pe_{\text{d(f)}}/30)]$. Liquid fuel transport properties were used for calculating $Pe_{\text{d(f)}}$. This model can predict the droplet average surface temperature, but not the distribution of temperature inside droplets. In our case, however, we are primarily interested in the accurate prediction of the former temperature, which controls droplet evaporation. Hence, the applicability of this model can be justified.

The aforementioned classification of the models was suggested based on the assumption that droplet heating is driven by convection. However, it can be equally applied to the case when the contribution of radiation is to be taken into account. The contribution of radiation is particularly important in the case when fresh droplets are injected into the burning gas in diesel engines. The temperature of gas in this case can exceed 2500 K [14–16]. So far the modelling of droplet convective and radiative heating, taking into account its finite effective thermal conductivity, has been performed based on the numerical simulation of the underlying equations. In this paper, the results of an analytical study of these processes will be presented. The approach presented in this paper is complementary to the one based on the assumption about the parabolic temperature profile distribution inside droplets [17,18]. The latter approach is more accurate than the one based on the assumption of no temperature gradient inside droplets, but less accurate than the one considered in this paper.

The previously suggested analytical solutions of the heat conduction equation in a sphere were limited to the case when the convection heat transfer coefficient was constant, and the heat source depended on time, but spacially homogeneous [20]. A number of analytical solutions for specific heat source distributions in a sphere are presented in [19], but no convection has been accounted for. The analytical solutions discussed in this paper are generalisations of the results reported in [19–22]. At first the explicit solution of the problem with constant heat transfer coefficient, but arbitrary distribution of radiative heat inside droplets, and arbitrary initial temperature distribution inside droplets, is constructed in the form of a convergent series. This solution is used as an auxiliary tool to solve the problem with the time-dependent heat transfer coefficient. The latter problem is reduced to the solution of an integral equation. This solution is unique and can be obtained numerically. The numerical algorithm is discussed. An approximate solution of the integral equation is obtained using the perturbation method for the case of almost constant heat transfer coefficient. An arbitrary initial distribution of temperature inside droplets is assumed. The effect of evaporation is taken into account via a non-zero time derivative of droplet radius in the enthalpy equation. The solution, however, is based on the assumption that the changes in droplet surface area are negligibly small. This assumption is justified when the time interval is small, while the latent heat of evaporation is large. Its range of applicability is investigated. The contribution of the radiation term is calculated using the simplified model developed by Dombrovsky and Sazhin [23,24]. The solution for the constant heat transfer coefficient is applied to the problem of fuel droplet heating in diesel engines.

The basic equations and approximations used in our analysis are discussed in Section 2. The solutions of the heat conduction equation are presented in Section 3. The application of one of the solutions to the problem of heating of diesel fuel droplets, is discussed in Section 4. The main results of the paper are summarised in Section 5.

2. Basic equations and approximations

Assuming that the temperature distribution inside a droplet (T) is spherically symmetrical the transient heat conduction equation inside this droplet can be written as [19,20]

$$c_{\text{l}}\rho_{\text{l}}\frac{\partial T}{\partial t} = k_{\text{l}}\left(\frac{\partial^2 T}{\partial R^2} + \frac{2}{R}\frac{\partial T}{\partial R}\right) + P_{\text{l}}(R), \tag{1}$$

where c_{l}, ρ_{l} and k_{l} are the liquid specific heat capacity, density and thermal conductivity respectively (assumed to be constant), R is the distance from the centre of the sphere, t is time and $P_{\text{l}}(R)$ is the power generated in unit volume inside the droplet due to external radiation.

If the droplet is heated by convection from the surrounding gas, and cooled down due to evaporation, the energy balance equation at the droplet surface can be written as

$$h(T_{\text{g}} - T_{\text{s}}) = -\rho_{\text{l}}L\dot{R}_{\text{d}} + k_{\text{l}}\left.\frac{\partial T}{\partial R}\right|_{R=R_{\text{d}}}, \tag{2}$$

where $h = h(t)$ is the convection heat transfer coefficient (time dependent in the general case), R_{d} is the droplet's radius, T_{g} is the gas ambient temperature, T_{s} is the droplet's surface temperature, L is the specific heat of evaporation. We took into account that $\dot{R}_{\text{d}} < 0$ during the evaporation process. Eq. (2) can be considered as a boundary condition for Eq. (1) at $R = R_{\text{d}}$. This needs to be complemented by the boundary condition at $R = 0$: $\left.\frac{\partial T}{\partial R}\right|_{R=0} = 0$, and the intial condition $T(t = 0) = T_0(R)$.

Introducing the normalised radius $r = R/R_{\text{d}}$, Eq. (1) can be rewritten as

$$\frac{\partial T}{\partial t} = \kappa\left(\frac{\partial^2 T}{\partial r^2} + \frac{2}{r}\frac{\partial T}{\partial r}\right) + P(r), \tag{3}$$

where

$$\kappa = \frac{k_l}{c_l \rho_l R_d^2},$$

$$P(r) = P_l(rR_d)/(c_l\rho_l) = \left[\frac{3\pi}{R_d}\int_{\lambda_1}^{\lambda_2} w(r,\lambda) Q_a B_\lambda(T_{ext})\,d\lambda\right] \Big/ (c_l\rho_l),$$

$B_\lambda(T_{ext})$ is the Planck function defined as

$$B_\lambda(T_{ext}) = \frac{C_1}{\pi\lambda^5[\exp(C_2/(\lambda T_{ext})) - 1]},$$

$C_1 = 3.742 \times 10^8$ W μm^4/m^2, $C_2 = 1.439 \times 10^4$ μm K, λ is the wavelength in μm. T_{ext} is assumed to be constant. Q_a is the efficiency factor of absorption which is estimated as [23,25]

$$Q_a = \frac{4n}{(n+1)^2}[1 - \exp(-2a_\lambda R_d)],$$

$w(r)$ is the normalised spectral power of radiation per unit volume absorbed inside the droplet [23], $a_\lambda = 4\pi\kappa_\lambda/\lambda$ is the liquid fuel absorption coefficient, n is the refractive index, λ_1 and λ_2 describe the spectral range of thermal radiation which contributes to droplet heating.

Eq. (2) can be rearranged to

$$T_{eff} - T_s = \frac{k_l}{hR_d}\frac{\partial T}{\partial r}\bigg|_{r=1}, \tag{4}$$

where $T_{eff} = T_g + \frac{\rho_l L \dot{R}_d}{h}$. Eq. (4) is complemented by the boundary condition at $r = 0$ and the corresponding initial condition mentioned above.

T_{eff} is time dependent in the general case to account for the effect of droplet evaporation and gas cooling. Although we take into account non-zero $\dot{R}_d$ due to evaporation, we assume that R_d is constant in all terms except in the definition of T_{eff}. This assumption would certainly be not acceptable if we attempted to describe the whole process of droplet evaporation by a single analytical formula. Our solutions, however, are suggested with a view of incorporation into a CFD code, where it will be applied over relatively small time steps. Due to the large value of the coefficient $\rho_l L/h$, the correction to T_g leading to T_{eff} can be justified even if the solutions are considered over small time intervals. In the realistic situation the temperature dependence of ρ_l needs to be taken into account. This would lead to the initial increase, rather than decrease of droplet radii despite the effect of evaporation [5].

The value of $\dot{R}_d$ is controlled by fuel vapour diffusion from the droplet surface [3]:

$$\dot{R}_d = -\frac{k_g \ln(1 + B_M)}{\rho_l c_{pg} R_d}, \tag{5}$$

where $B_M = Y_{fs}/(1 - Y_{fs})$ is the Spalding number, Y_{fs} is the mass fraction of fuel vapour near the droplet surface:

$$Y_{fs} = \left[1 + \left(\frac{p}{p_{fs}} - 1\right)\frac{M_a}{M_f}\right]^{-1}, \tag{6}$$

p and p_{fs} are ambient pressure and the pressure of saturated fuel vapour near the surface of droplets respectively, M_a and M_f are molar masses of air and fuel; p_{Fs} can be calculated from the Clausius–Clapeyron equation presented in the form [26,27]:

$$p_{Fs} = \exp\left[a - \frac{b}{T_s - 43}\right], \tag{7}$$

a and b are constants to be specified for specific fuels, p_{Fs} is in kPa.

A more general kinetic approach to the problem is based on the solution of the Boltzmann equation in the Knudsen layer surrounding the droplet. In diesel engines this kinetic model predicts up to 5–10% larger evaporation times when compared with the evaporation times predicted by the hydrodynamic model on which Eq. (5) is based [28]. Analysis of the kinetic model is beyond the scope of this paper.

Eqs. (3) and (5) can be solved by iterations. At first one can assume that $T_s = T_{s0}$ in Eq. (7) and obtain the solution of Eq. (3) as $T_s = T_{s1}(t)$. Then this solution is substituted into Eq. (7). When T_s approaches the boiling temperature T_b then the assumptions $Y_{fs} \ll 1$ and $R_d = \text{const}$ become no longer applicable. The solution of the problem in this case is beyond the scope of this paper (see [29]).

Introduction of the new variable $u = Tr$ allows us to rewrite Eq. (3) as

$$\frac{\partial u}{\partial t} = \kappa\frac{\partial^2 u}{\partial r^2} + \widetilde{P}(r) \tag{8}$$

with the boundary and initial conditions:

$$\left.\begin{array}{ll} \dfrac{\partial u}{\partial r} + H(t)u = M(t) & \text{when } r = 1 \\ u = 0 & \text{when } r = 0 \\ u(t=0) = rT_0(rR_d) \equiv \widetilde{T}_0(r) & \text{when } 0 \leqslant r \leqslant 1 \end{array}\right\} \tag{9}$$

where

$$H(t) = \frac{h(t)R_d}{k_l} - 1, \quad M(t) = \frac{h(t)T_{eff}(t)R_d}{k_l}, \quad \widetilde{P}(r) = rP(r).$$

3. Analytical solutions

3.1. Case $h(t) = const$

At first we consider the case $h(t) \equiv h = \text{const}$. Hence, $H(t) \equiv h_0 = (hR_d/k_l) - 1 = \text{const}$. Introducing a new parameter $\mu_0(t) = hT_{eff}(t)R_d/k_l$ we can rewrite Eqs. (9) as

$$\left.\begin{array}{ll} \dfrac{\partial u}{\partial r}+h_0u=M(t)=\mu_0(t) & \text{when } r=1\\ u=0 & \text{when } r=0\\ u(t=0)=rT_0(rR_{\rm d})\equiv\widetilde{T}_0(r) & \text{when } 0\leqslant r\leqslant 1 \end{array}\right\} \tag{10}$$

Remembering that $h_0>-1$ let us look for the solution of Eq. (8) in the form:

$$u(r,t)=\frac{1}{1+h_0}r\mu_0(t)+W(r,t). \tag{11}$$

Having substituted function (11) into Eq. (8) we find the equation for W:

$$\frac{\partial W}{\partial t}=\kappa\frac{\partial^2 W}{\partial r^2}+\widetilde{P}(r)-\frac{r}{1+h_0}\frac{{\rm d}\mu_0(t)}{{\rm d}t} \tag{12}$$

with the boundary and initial conditions:

$$\left.\begin{array}{l} W|_{r=0}=\left(\dfrac{\partial W}{\partial r}+h_0W\right)\Big|_{r=1}=0,\\ W|_{t=0}=\widetilde{T}_0(r)-\dfrac{r}{1+h_0}\mu_0(0). \end{array}\right\} \tag{13}$$

The solution of Eq. (12) subject to (13) can be presented as (see Appendix A)

$$W(r,t)=\sum_{n=1}^{\infty}\left\{\frac{p_n}{\kappa\lambda_n^2}+\exp[-\kappa\lambda_n^2t]\left(q_n+f_n\mu_0(0)-\frac{p_n}{\kappa\lambda_n^2}\right)+f_n\int_0^t\frac{{\rm d}\mu_0(\tau)}{{\rm d}\tau}\exp[-\kappa\lambda_n^2(t-\tau)]{\rm d}\tau\right\}\sin\lambda_nr, \tag{14}$$

where p_n, q_n, f_n and λ_n are defined by Eqs. (A.8) and (A.3), and

$$u(r,t)=\frac{1}{1+h_0}r\mu_0(t)+\sum_{n=1}^{\infty}\left\{\frac{p_n}{\kappa\lambda_n^2}+\exp[-\kappa\lambda_n^2t]\left(q_n+f_n\mu_0(0)-\frac{p_n}{\kappa\lambda_n^2}\right)+f_n\int_0^t\frac{{\rm d}\mu_0(\tau)}{{\rm d}\tau}\exp[-\kappa\lambda_n^2(t-\tau)]{\rm d}\tau\right\}\sin\lambda_nr. \tag{15}$$

Remembering (A.8) and the definition of u, the final solution of Eq. (3) can presented as

$$T(r,t)=\frac{1}{r}\sum_{n=1}^{\infty}\left\{\frac{p_n}{\kappa\lambda_n^2}+\exp[-\kappa\lambda_n^2t]\left(q_n-\frac{p_n}{\kappa\lambda_n^2}\right)-\frac{\sin\lambda_n}{\|v_n\|^2\lambda_n^2}\mu_0(0)\exp[-\kappa\lambda_n^2t]-\frac{\sin\lambda_n}{\|v_n\|^2\lambda_n^2}\int_0^t\frac{{\rm d}\mu_0(\tau)}{{\rm d}\tau}\exp[-\kappa\lambda_n^2(t-\tau)]{\rm d}\tau\right\}\times\sin\lambda_nr+T_{\rm eff}(t). \tag{16}$$

We took into account that $T_{\rm eff}(t)=k_{\rm l}\mu_0(t)/(hR_{\rm d})$. If $T_0(r)$ is twice differentiable, then the series in (14)–(16) converge absolutely and uniformly for all $t\geqslant 0$ and $r\in[0,1]$ since

$$|p_n|<\text{const},\quad |q_n|<\frac{\text{const}}{\lambda_n^2},$$
$$|\sin\lambda_nr|\leqslant 1,\quad \exp(-\kappa_0\lambda_n^2t)\leqslant 1,$$

and $\lambda_n^{-2}<n^{-2}$ for $n>1$. It can be shown that $\lambda_n>\pi(n-1)$. Hence, for $n>1$:

$$\lambda_n>n\pi\left(1-\frac{1}{n}\right)>n\pi/2>n. \tag{17}$$

When $\mu_0=\text{const}$, $P(r)=0$, $T_{\rm eff}=\text{const}$ and $k_{\rm l}\to\infty$ Eq. (16) reduces to [30]

$$T_{\rm s}=T_{\rm g}+(T_{\rm s0}-T_{\rm g})\exp\left(-\frac{3ht}{c_{\rm l}\rho_{\rm l}R_{\rm d}}\right), \tag{18}$$

where $T_{\rm s}(t=0)=T_{\rm s0}$.

The same expression could be obtained directly from the energy balance at the surface of the droplet, assuming that there is no temperature gradient inside the droplet (model 1):

$$\frac{4}{3}\pi R_{\rm d}^3\rho_{\rm l}c_{\rm l}\frac{{\rm d}T_{\rm s}}{{\rm d}t}=4\pi R_{\rm d}^2h(T_{\rm g}-T_{\rm s}). \tag{19}$$

3.2. Case $h(t)\neq$ const (general case)

Let us assume that

$$H(t)=h_0+h_1(t), \tag{20}$$

where $h_0=\text{const}\neq-1$ and $h_1(t)$ is an arbitrary function of time. This enables us to use the results obtained in the previous section for the general analysis. If $h_0=0$ then $H(t)=h_1(t)$.

Having substituted (20) into conditions (9) we can generalise conditions (10) as

$$\left.\begin{array}{ll} \dfrac{\partial u}{\partial r}+h_0u=-h_1(t)u+\mu_0(t)\equiv\mu_{\rm g0}(t) & \text{when } r=1\\ u=0 & \text{when } r=0\\ u(t=0)=rT_0(rR_{\rm d})\equiv\widetilde{T}_0(r) & \text{when } 0\leqslant r\leqslant 1 \end{array}\right\}. \tag{21}$$

If $\mu_{\rm g0}(t)$ is a known function then conditions (21) reduce to conditions (10) with $\mu_0(t)$ replaced by $\mu_{\rm g0}(t)$. The analytical solution of the problem would then be given by series (15) with $\mu_0(t)$ replaced by $\mu_{\rm g0}(t)$. Integration of the last term of this equation by parts allows us to write

$$u(r,t)=\frac{r\mu_{g0}(t)}{1+h_0}+U(r,t)+\sum_{n=1}^{\infty}\left\{f_n\mu_{g0}(t)-\kappa\lambda_n^2 f_n \times\int_0^t\mu_{g0}(\tau)\exp[-\kappa\lambda_n^2(t-\tau)]\,d\tau\right\}\sin\lambda_n r, \quad (22)$$

where

$$U(r,t)=\sum_{n=1}^{\infty}\left\{\frac{p_n}{\kappa\lambda_n^2}+\exp[-\kappa\lambda_n^2 t]\left(q_n-\frac{p_n}{\kappa\lambda_n^2}\right)\right\}\sin(\lambda_n r).$$

Remembering (A.7) and (A.8) we can rewrite (22) as

$$u(r,t)=U(r,t)-\int_0^t\mu_{g0}(\tau)G(t-\tau,r)\,d\tau, \quad (23)$$

where

$$G(t,r)=\kappa\sum_{n=1}^{\infty}\lambda_n^2 f_n\exp[-\kappa\lambda_n^2 t]\sin\lambda_n r =-\kappa\sum_{n=1}^{\infty}\frac{\sin\lambda_n}{\|v_n\|^2}\exp[-\kappa\lambda_n^2 t]\sin\lambda_n r. \quad (24)$$

One can show that $G(t,r)$ is continuous at $t>0$. For $t\to+0$ the following inequality holds:

$$|G(t,r)|<\frac{c}{\sqrt{t}} \quad (25)$$

uniformly with respect to $r\in[0,1]$ (see Appendix B).

Remembering that $\mu_{g0}(t)=M(t)-h_1(t)u(1,t)$ we can rewrite (23) in the form:

$$u(r,t)=U(r,t)-\int_0^t[M(\tau)-h_1(\tau)u(1,\tau)]G(t-\tau,r)\,d\tau. \quad (26)$$

This formula gives us an integral representation of the solution of the problem (8), (21). For $r=1$ integral representation (26) reduces to the integral equation for the function $u(1,t)$:

$$u(1,t)=U(1,t)-\int_0^t[M(\tau)-h_1(\tau)u(1,\tau)]G(t-\tau,1)\,d\tau, \quad (27)$$

where

$$G(t,1)=-\kappa\sum_{n=1}^{\infty}\frac{\sin^2\lambda_n}{\|v_n\|^2}\exp[-\kappa\lambda_n^2 t] =-2\kappa\sum_{n=1}^{\infty}\frac{\lambda_n^2}{h_0^2+h_0+\lambda_n^2}\exp[-\kappa\lambda_n^2 t]. \quad (28)$$

We took into account that

$$\sin^2\lambda_n=\frac{1}{1+\cot^2\lambda_n}=\frac{1}{1+(h_0/\lambda_n)^2}=\frac{\lambda_n^2}{\lambda_n^2+h_0^2}.$$

If $h_0=0$ then $G(t,1)=-2\kappa\sum_{n=1}^{\infty}\exp[-\kappa\lambda_n^2 t]$, where $\lambda_n=\pi(n-(1/2))$. As shown in Appendix B, the kernel $G(t,1)$ is continuous if $t\neq 0$. It has integrable singularity $G(t,1)\propto t^{-1/2}$ when $t\to+0$. The integral equation (27) is the so-called Volterra integral equation of the second kind. This equation has a unique solution, although this solution cannot be found in an explicit form. The scheme of its numerical solution is described in Appendix C. Once the solution of this equation has been found we can substitute it into integral representation (26) and find the required solution of the initial and boundary value problem (8), (21). The required distribution of T is found as $T=u/r$. In the case when $h_1(t)=0$ this solution reduces to that given by (16). To simplify the numerical solution of the equation it is reasonable to take $h_0=0$. In this case $\lambda_n=\pi(n-(1/2))$ and $\|v_n\|^2=1/2$ in all equations.

3.3. Case of almost constant $h(t)$

In the case of almost constant $h(t)$ we can use representation (20) and assume that $h_1(t)=\epsilon\eta(t)$, where ϵ is a small parameter. In this case the perturbation theory can be applied to the analysis of Eq. (27). We look for the solution $u(1,t)$ of this equation in the form:

$$u(1,t)\equiv v(t)=v_0(t)+\epsilon v_1(t)+\epsilon^2 v_2(t)+\cdots=\sum_{j=0}^{\infty}\epsilon^j v_j(t). \quad (29)$$

The substitution of series (29) into the integral equation (27) gives

$$\sum_{j=0}^{\infty}\epsilon^j v_j(t)=U(1,t)-\int_0^t\left[M(\tau)-\eta(\tau)\sum_{j=0}^{\infty}\epsilon^{j+1}v_j(\tau)\right]\times G(t-\tau,1)\,d\tau. \quad (30)$$

The terms with the same powers of ϵ in the left-hand and the right-hand sides of Eq. (30) should be equal. Hence, Eq. (30) reduces to the following system of equations:

$$\left.\begin{aligned}&\epsilon^0: v_0(t)=U(1,t)-\textstyle\int_0^t M(\tau)G(t-\tau,1)\,d\tau,\\ &\epsilon^1: v_1(t)=\textstyle\int_0^t\eta(\tau)v_0(\tau)G(t-\tau,1)\,d\tau,\\ &\vdots\\ &\epsilon^j: v_j(t)=\textstyle\int_0^t\eta(\tau)v_{j-1}(\tau)G(t-\tau,1)\,d\tau,\end{aligned}\right\} \quad (31)$$

Formulae (31) allow us to find all functions $v_j(t)$ step-by-step. Substitution of these functions into series (29) gives the solution of the integral equation (27) in the form of a power series in ϵ. One can show that this series converges absolutely and uniformly for $t\in[0,t_0]$, if t_0 is a fixed number and ϵ (depending on t_0) is small enough (see Appendix D). Substitution of this solution into integral representation (26) gives the solution of the problem (8) and (21) for $u(r,t)$. The solution of the original problem for $T(r,t)$ is $T(r,t)=u(r,t)/r$. Keeping

only linear terms in the series (29) we obtain the approximate solution of Eq. (27) with accuracy $O(\epsilon^2)$:

$$u(1,t) = U(1,t) - \int_0^t M(\tau)G(t-\tau,1)\,d\tau + \epsilon\int_0^t \eta(\tau)v_0(\tau)G(t-\tau,1)\,d\tau. \quad (32)$$

4. Application

The theory developed in the previous sections is applied to a specific problem of heating fuel droplets in diesel engines [5,6]. We take gas pressure $p = 6$ MPa, $T_g = T_{ext} = 1000$ K and 2000 K, $k_g = 0.061$ W/(m K), $T_{s0} = 300$ K, $\rho_l = 846$ kg/m^3, $M_a = 28.97$ kg/kmol, $M_f = 198$ kg/kmol, $k_l = 0.14$ W/(m K), $c_l = 2$ kJ/(kg K), $a = 15.5274$, $b = 5383.59$, $L = 254$ kJ/kg, $R_d = 50$ μm and $R_d = 25$ μm [26,27,31,32]. Droplets are assumed to be stationary ($Re_d = 0$). The generalisation of the results to the case of moving droplets would require the modification of h and introducing k_{eff} instead of k_l as discussed in the Introduction. We consider the case $h = \text{const}$ which allows us to focus the analysis on formula (16). This formula needs to be used in combination with formula (5) for $\dot{R}_d$ and remembering the definition of T_{eff}.

We start with calculating the radial distribution of the radiation power absorbed inside droplets. The plots for κ_λ and the approximations for $w(r)$ presented in Appendix E have been used. We restrict our analysis to the unboiled low sulfur ESSO AF1313 diesel fuel used in cars. Analysis of other types of fuel leads to essentially similar results. The plots of $P(r)$ versus r for $R_d = 50$ μm, $R_d = 25$ μm and $T_g = T_{ext} = 1000$ K, $T_g = T_{ext} = 2000$ K are shown in Fig. 1. The shape of these curves is rather similar to the one reported in [23], where slightly less accurate results of measurement of κ_λ of diesel fuel and the simplified approximation of κ_λ have been used. The difference between the values of κ_λ predicted by [23] and our calculations did not exceed 9%. A typical feature of all plots is the presence of two maxima in $P(r)$: one near the surface of the droplet, and another at $r = 1/n \approx 1/1.46 = 0.68$. The discontinuity of the slope at $r = 1/n$ is related to the fact that all rays entering the droplet from outside, will concentrate in the cone with the half angle $\theta = \sin^{-1}(1/n)$ after refraction at the surface. The spheres of radii $r = 1/n$ are the maximal spheres inside this cone. The results show that increasing the size of droplet radii leads to an increase in the value of $P(r)$. Hence, larger droplets are expected to absorb more thermal radiation due to their size, and also to have a larger concentration of absorbed radiation. These results are consistent with the prediction of the overall absorption efficiency factor reported in [2]. As expected,

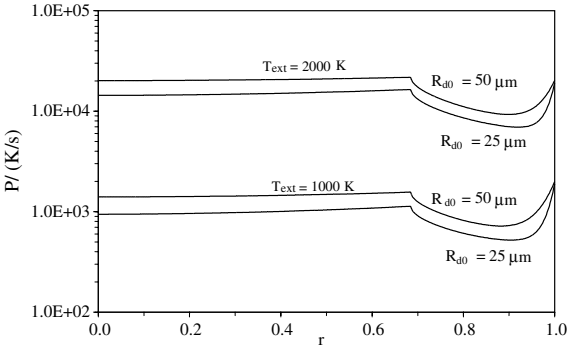

Fig. 1. Plots of thermal radiation power density absorbed by diesel fuel droplets versus normalised radius. Droplet radii are taken equal to 25 and 50 μm; external temperatures are taken equal to 1000 and 2000 K (indicated near the curves). The curves are presented for unboiled low sulfur ESSO AF1313 diesel fuel used in cars (DF1 fuel).

the increase in external temperature leads to a considerable increase of $P(r)$.

The application of formula (16) requires truncation of the series. As will be shown later, this series converges rather quickly. As a starting point, however, we take 25 terms of this series (the higher-order terms are in most cases less than the round-up errors of the computer). Assuming $T_{eff} = T_{ext} = \text{const} = 2000$ K, $T(r, t = 0) = T_d = 300$ K and $R_d = 50$ μm the plots of $T(r,t)$ versus r are presented in Fig. 2 for $t = 0.01$, 0.1, 1 and 5 ms both with and without radiation. As follows from this figure, the effect of radiation leads to a small (about 10%) increase in the droplet temperature at $t = 5$ ms. At shorter times this increase is smaller. Note that radiation leads to an increase in temperature throughout the

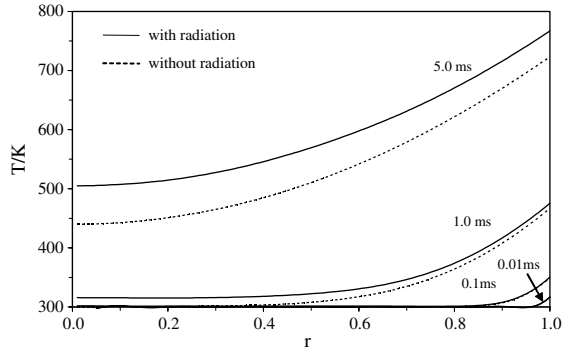

Fig. 2. Plots of droplet temperature versus normalized radius r for various times (indicated near the curves). Droplet radius and gas and external temperatures are taken equal 50 μm and 2000 K respectively. Curves for the cases when thermal radiation was ignored (dashed) and taken into account (solid) are presented.

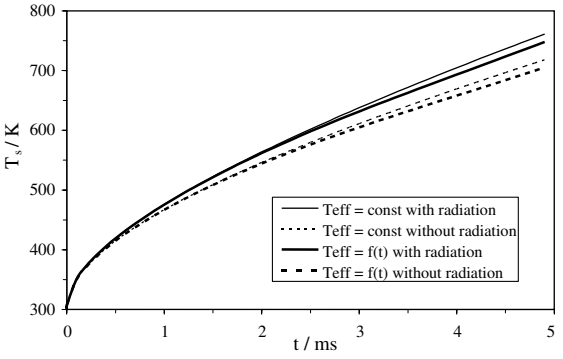

Fig. 3. Plots of droplet surface temperature versus time for the case when $T_{\text{eff}} = \text{const}$ (zeroth iteration) and $T_{\text{eff}} = T_{\text{eff}}(t)$ (first iteration). Droplet radius and gas and external temperatures are taken equal 50 μm and 2000 K respectively. Curves for the cases when thermal radiation was ignored (dashed) and taken into account (solid) are presented.

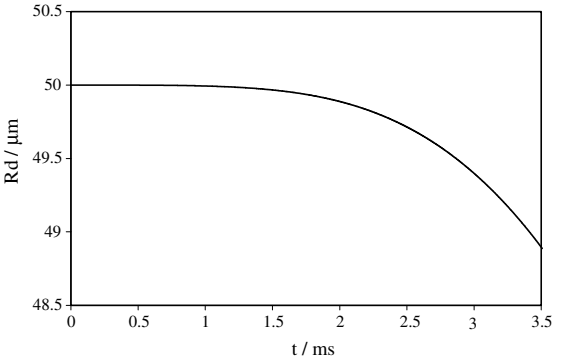

Fig. 4. Plots of droplet radius versus time for the case when the initial droplet radius and gas and external temperatures are equal 50 μm and 2000 K respectively. Effects of thermal radiation are taken into account.

whole droplet as expected. At shorter times, droplet temperature increases in the immediate vicinity of its' surface only.

The plots of droplet surface temperatures versus time for the same values of gas temperature, initial droplet temperature and droplet radii, as in Fig. 2, are shown in Fig. 3. Similarly to Fig. 2, the plots taking and not taking into account the effects of radiation are presented. In contrast to Fig. 2, the cases $T_{\text{eff}} = T_{\text{ext}} = \text{const}$ (zeroth iteration) and $T_{\text{eff}} = T_{\text{eff}}(t)$, but $T_{\text{ext}} = \text{const}$ (first iteration) are presented. The plots for the second and higher iterations are practically indistinguishable from those for the first iteration.

In agreement with Fig. 2, Fig. 3 shows that the effect of thermal radiation leads to a noticeable (up to about 10%) increase in droplet surface temperature. This effect is even more pronounced for higher gas temperatures. Comparing the predictions of the zeroth and first approximations, we can see that at $t \leqslant 2$ ms they are practically undistinguishable. This means that the effects of droplet evaporation at $t \leqslant 2$ ms can be ignored. This is confirmed by Fig. 4 where the plot of R_{d} versus time, as predicted by (5), is shown. As follows from Fig. 4, the decrease in droplet radius at $t \leqslant 2$ ms is less than 0.3%. This justifies our approximation that $R_{\text{d}} = \text{const}$.

Now we can investigate the influence of the number of terms in the series taken on the accuracy of the predicted values of droplet temperature. The plots of $T(r)$ versus r for $t = 1$ ms, $T_{\text{eff}} = T_{\text{ext}} = \text{const} = 2000$ K, $T(r, t = 0) = T_{\text{d}} = 300$ K, $R_{\text{d0}} = 50$ μm and several numbers of terms in the series taken are shown in Fig. 5. The effect of radiation was taken into account. As can be seen in this figure, the prediction of the series with just three terms is practically indistinguishable from the prediction of the series with 25 terms. This agrees with

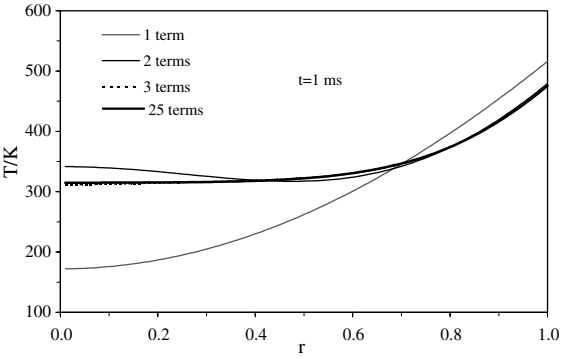

Fig. 5. Plots of droplet temperature versus normalized radius r for $t = 1$ ms. The plots refer to the case when 1, 2, 3 and 25 terms in the series are taken. Droplet radius and gas and external temperatures are taken equal 50 μm and 2000 K respectively. The contribution of thermal radiation was taken into account.

the prediction of Table 1, where the results of our analysis of the number of terms required for $T_{\text{eff}} = T_{\text{ext}} = 2000$ K and the average errors are shown.

The line 'number of terms' indicates the number of terms required in order for the average error in the estimate of the series does not exceed 1%. The actual average error is indicated in the same table. Note that if we consider the errors in the estimate of T_{s} rather than average errors, then the number of terms required to meet the same criterion would be slightly different. For $R_{\text{d}} = 50$ μm and $t = 0.01$, 0.1, 1 and 5 ms these numbers would be 12, 5, 2 and 1 respectively. For $R_{\text{d}} = 25$ μm and $t = 0.01$, 0.1, 1 and 5 ms these numbers would be 8, 3, 1 and 1 respectively. As follows from this table, the required number of terms increases with decreasing t and increasing R_{d}.

Table 1

	R_{d0} (μm)							
	50				25			
t (ms)	0.01	0.1	1	5	0.01	0.1	1	5
Number of terms	6	5	3	2	6	4	2	2
Average error (%)	0.94	0.61	0.14	0.16	0.63	0.22	0.07	0.02

Table 2

	R_{d0} (μm)							
	50				25			
t (ms)	0.01	0.1	1	5	0.01	0.1	1	5
Number of terms	3	2	2	2	2	2	2	2
Average error (%)	0.38	0.92	0.45	0.14	0.05	0.07	0.04	0.02

In Table 2 the results similar to those shown in Table 1, but for the initial distribution of droplet temperature predicted by Eq. (16) for $t = 1$ ms are shown. This can approximate further heating of an initially preheated droplet. As can be seen from this table, the number of terms in the series required for practical applications is noticeably less that in the case of modelling of heating of a cold droplet. As in the case shown in Table 1, the number of terms required decreases with decrease of droplet radius. In fact if droplet radii less than 10 μm are considered then just one term in the series would be sufficient to ensure the error of less than 1%. If we consider the errors in the estimate of T_s rather than average errors, then the number of terms required to get an error of less than 1% would be slightly different. For $R_d = 50$ μm and $t = 0.01$, 0.1, 1 and 5 ms these numbers would be 3, 2, 2 and 1 respectively. For $R_d = 25$ μm and all times one term would be sufficient. This has an important implication when we incorporate the results into a CFD code. If we ignore the effects of very initial heating of droplets, then three terms of the series in (16) would be more than enough to ensure that the error of calculations is well below 1%.

Plots similar to those shown in Figs. 2–5 can be shown for other values of T_{eff} and T_{ext} and R_d. One of the most important characteristics following from these curves would be the upper time limit (t_{up}) over which the approximations $T_{eff} = \text{const}$ and $R_d = \text{const}$ are valid. The values of t_{up} for various T_{eff} and R_d are shown in Table 3. It was assumed that $T_{eff} = T_{ext}$.

The values of t_{up} have been estimated as those t for which the decrease in R_d have not exceeded 0.2%. As follows from this table, the values of t_{up} decrease with decreasing R_d and increasing T_{eff}. Note that even in the most unfavourable situation the values of t_{up} are large enough to play an important role in the process of droplet heating in diesel engines [5,6]. Note that taking into account the contribution of $\dot{R}_d$ leads to a much larger decrease in T_s than in R_d as expected. This provides additional support to our assumption that $R_d = \text{const}$, but $\dot{R}_d \neq 0$.

Table 3

	R_{d0} (μm)			
	50		25	
T_{eff} (K)	1000	2000	1000	2000
t_{up} (ms)	6.4	2.0	1.6	0.5
Decrease in predicted T_{eff} (%)	1.19	0.99	1.19	1.71

5. Conclusions

Analytical solutions of the heat conduction equation inside a spherical droplet have been suggested. The droplet has been assumed to be heated by convection and radiation from the surrounding hot gas—a situation typical in many engineering applications. Initial droplet evaporation, the effects of time dependent gas temperature and the convection heat transfer coefficient have been taken into account. Three approximations for the convection heat transfer coefficient have been considered. Firstly, this coefficient has been assumed constant and an explicit formula for the time dependent distribution of temperature inside droplets has been derived. Secondly, the general case of time dependent convection heat transfer coefficient has been considered. In this case the solution of the original differential equation has been reduced to the solution of the Volterra integral equation of the second kind. A numerical scheme for the solution of this equation has been suggested. Thirdly, the case of almost constant convection heat transfer coefficient has been considered. In this case the problem has been solved using the perturbation theory. A set of solutions

corresponding to ascending approximations have been obtained.

Results referring to the case of constant convection heat transfer coefficient have been applied to a typical problem of fuel droplet heating in a diesel engine. Results of the measurements of the index of absorption of four different types of diesel fuels have been presented. Only results referring to low-sulfur ESSO AF1313 diesel fuel used in cars have been used in the analysis. Results referring to other types of diesel fuel are expected to lead to similar conclusions. It has been shown that the effects of radiation lead to a noticeable increase in droplet temperature, especially at larger times and larger droplet radii. The distribution of temperature inside droplets has been shown to be different from constant values, as assumed in the isothermal model. This implies that finite thermal conductivity of fuel droplets and the effects of radiation need to be taken into account when modelling droplet heating in diesel engines. It has been shown that the range of times when the model is applicable decreases with decreasing droplet radii and increasing ambient gas temperature.

Acknowledgements

The authors are grateful to the Royal Society and EPSRC (grant GR/R82920/01) for the financial support of this project.

Appendix A. Solution of Eq. (12)

We look for the solution of Eq. (12) subject to (13) in the form:

$$W(r,t)=\sum_{n=1}^{\infty}c_n(t)v_n(r), \tag{A.1}$$

where functions $v_n(r)$ form the full set of non-trivial solutions of the equation:

$$\frac{\mathrm{d}^2v}{\mathrm{d}r^2}+\lambda^2v=0 \tag{A.2}$$

subject to the boundary condition $v|_{r=0}=\left(\frac{\mathrm{d}v}{\mathrm{d}r}+h_0v\right)\big|_{r=1}=0$. The general solution of Eq. (A.2) $v(r)=A\cos\lambda r+B\sin\lambda r$ satisfies the boundary condition when $A=0$ and

$$\lambda\cos\lambda+h_0\sin\lambda=0. \tag{A.3}$$

The solution of Eq. (A.3) gives a set of positive eigenvalues λ_n numbered in ascending order ($n=1,2,\ldots$). If $h_0=0$, then $\lambda_n=\pi\left(n-\frac{1}{2}\right)$. Assuming that $B=1$, expressions for eigenfunctions v_n can be written as $v_n(r)=\sin\lambda_n r$ ($n=1,2,\ldots$). The value of B is implicitly accounted for by the coefficients $c_n(t)$ in series (A.1). The functions $v_n(r)$ form a full set of eigenfunctions which are orthogonal for $r\in[0,1]$. The orthogonality of functions v_n follows from the relation:

$$\int_0^1 v_n(r)v_m(r)\,\mathrm{d}r=\delta_{nm}\|v_n\|^2, \tag{A.4}$$

where

$$\delta_{nm}=\begin{cases}0, & n\neq m,\\ 1, & n=m,\end{cases}\quad \|v_n\|^2=\frac{1}{2}\left(1-\frac{\sin 2\lambda_n}{2\lambda_n}\right)=\frac{1}{2}\left(1+\frac{h_0}{h_0^2+\lambda_n^2}\right).$$

The eigenvalue $\lambda_0=0$ describes the trivial eigenfunction $v_0(r)=0$. The orthogonality of v_n allows us to expand known functions in Eqs. (12) and (13) in the series:

$$\widetilde{P}(r)=\sum_{n=1}^{\infty}p_nv_n(r), \tag{A.5}$$

$$\widetilde{T}_0(r)=\sum_{n=1}^{\infty}q_nv_n(r), \tag{A.6}$$

$$f(r)\equiv -r/(1+h_0)=\sum_{n=1}^{\infty}f_nv_n(r), \tag{A.7}$$

where

$$\left.\begin{aligned}p_n&=\frac{1}{\|v_n\|^2}\int_0^1\widetilde{P}(r)v_n(r)\,\mathrm{d}r,\quad q_n=\frac{1}{\|v_n\|^2}\int_0^1\widetilde{T}_0(r)v_n(r)\,\mathrm{d}r,\\ f_n&=\frac{1}{\|v_n\|^2}\int_0^1 f(r)v_n(r)\,\mathrm{d}r=-\frac{\sin\lambda_n}{\|v_n\|^2\lambda_n^2}.\end{aligned}\right\} \tag{A.8}$$

Having substituted series (A.1), (A.5) and (A.7) into Eq. (12), we obtain

$$\sum_{n=1}^{\infty}\left(\frac{\mathrm{d}c_n(t)}{\mathrm{d}t}+c_n(t)\kappa\lambda_n^2\right)v_n(r)=\sum_{n=1}^{\infty}\left(p_n+f_n\frac{\mathrm{d}\mu_0(t)}{\mathrm{d}t}\right)v_n(r). \tag{A.9}$$

Both sides of Eq. (A.9) are Fourier series of functions $v_n(r)$. Two Fourier series are equal if and only if their coefficients are equal. This implies that

$$\frac{\mathrm{d}c_n(t)}{\mathrm{d}t}+c_n(t)\kappa\lambda_n^2=p_n+f_n\frac{\mathrm{d}\mu_0(t)}{\mathrm{d}t}. \tag{A.10}$$

The initial condition for $c_n(t)$ follows from the initial condition for W: $c_n(0)=q_n+f_n\mu_0(0)$. The solution of (A.10), subject to this initial condition, can be written as

$$c_n(t)=\frac{p_n}{\kappa\lambda_n^2}+\exp[-\kappa\lambda_n^2t]\left(q_n+f_n\mu_0(0)-\frac{p_n}{\kappa\lambda_n^2}\right)+f_n\int_0^t\frac{\mathrm{d}\mu_0(\tau)}{\mathrm{d}\tau}\exp[-\kappa\lambda_n^2(t-\tau)]\mathrm{d}\tau. \tag{A.11}$$

Having substituted functions (A.11) and $v(r)$ into series (A.1) we obtain solution (14).

Appendix B. Estimate of $G(t,r)$ at $t\to 0$

Series (24) converges absolutely and uniformly to the continuous function for $(t,r)\in[\delta,\infty)\times[0,1]$ for any small $\delta>0$ since

$$\exp[-\kappa\lambda_n^2 t]<\exp[-\kappa n^2 t]\leqslant\exp[-\kappa n^2\delta] \tag{B.1}$$

(recall that $\lambda_n^2>n^2$ for $n>1$ according to inequalities (17)). Now we prove the estimate (25) for $t>0$. Inequality (B.1) allows us to write

$$|G(t,r)|\leqslant c_0\kappa\left\{1+\sum_{n=2}^{\infty}\exp[-\kappa n^2 t]\right\}\equiv\widetilde{G}(t), \tag{B.2}$$

where c_0 is a constant for which the condition $\|v_n\|^{-2}\leqslant c_0$ is satisfied. For example, if $h_0\geqslant 0$ we can take $c_0=2$ since $\|v_n\|^2\geqslant 1/2$. The sum $\sum_{n=2}^{\infty}\exp[-\kappa n^2 t]$ can be considered as a sum of areas of polygons of unit width placed under the curve $\exp[-\kappa y^2 t]$. This sum is less than the area under this curve. Hence,

$$\begin{aligned}\sum_{n=2}^{\infty}\exp[-\kappa n^2 t]&<\int_1^{\infty}\exp[-\kappa y^2 t]\mathrm{d}y\\&<\int_0^{\infty}\exp\left[-\kappa y^2 t\right]\mathrm{d}y\\&=\frac{1}{\sqrt{\kappa t}}\int_0^{\infty}\exp[-z^2]\mathrm{d}z=\frac{\sqrt{\pi}}{2\sqrt{\kappa t}}.\end{aligned} \tag{B.3}$$

Having substituted (B.3) into (B.2), we obtain

$$|G(t,r)|\leqslant\widetilde{G}(t)<c_0\kappa\left[1+\frac{\sqrt{\pi}}{2\sqrt{\kappa t}}\right]<\tilde{c}/\sqrt{t},\quad t\in(0,t_0] \tag{B.4}$$

for any fixed $t_0>0$. The new constant $\tilde{c}$ depends on t_0. Inequality (B.4) is equivalent to Inequality (25). It holds uniformly for $r\in[0,1]$.

Appendix C. Numerical solution of Eq. (27)

Let $\psi(t)\equiv u(1,t)$ and rewrite Eq. (27) as

$$\psi(t)=U(1,t)-\int_0^t[M(\tau)-h_1(\tau)\psi(\tau)]G(t-\tau,1)\,\mathrm{d}\tau. \tag{C.1}$$

We look for the solution of Eq. (C.1) for $t\in[0,\hat{t}]$, where $\hat{t}$ is a constant. Let $\Delta t=\hat{t}/N$ and $t_n=n\Delta t$, where N is the total number of timesteps, $n=0,1,\ldots,N$ is the number of the current timestep. Note that $t_0=0$ and $t_N=\hat{t}$. Discretisation of Eq. (C.1) gives

$$\begin{aligned}\psi(t_n)=U(1,t_n)-\sum_{j=1}^{n}\int_{t_{j-1}}^{t_j}[M(\tau)-h_1(\tau)\psi(\tau)]\\\times G(t_n-\tau,1)\,\mathrm{d}\tau,\end{aligned} \tag{C.2}$$

where $n=1,\ldots,N$. Note that $\psi(t_0)=\psi(0)=U(1,0)=\widetilde{T}_0(1)$ is a known constant.

The first $(n-1)$ integrals in this sum can be approximated as

$$\begin{aligned}&\int_{t_{j-1}}^{t_j}[M(\tau)-h_1(\tau)\psi(\tau)]G(t_n-\tau,1)\,\mathrm{d}\tau\\&\quad\approx\left\{M(\tau_j)-h_1(\tau_j)\frac{[\psi(t_j)+\psi(t_{j-1})]}{2}\right\}G(t_n-\tau_j,1)\Delta t,\end{aligned} \tag{C.3}$$

where $j=1,2,\ldots,n-1$, $\tau_j=t_j-\frac{1}{2}\Delta t$. Approximation (C.3) is valid since all functions in the integrand are continuous and we look for the solution in the class of continuous functions. The known functions are taken at $\tau=\tau_j$ (middle of the range $[t_{j-1},t_j]$), while the unknown functions are taken as the average of the values at the end points t_{j-1} and t_j.

The last term in the sum in Eq. (C.2) requires special investigation since the kernel $G(t_n-\tau,1)$ in the integrand becomes singular when $\tau\to t_n-0$ (see estimate (B.4)). All other functions in this integrand, including the unknown function $u(t)$ are assumed continuous. Hence, we can write

$$\begin{aligned}&\int_{t_{n-1}}^{t_n}[M(\tau)-h_1(\tau)\psi(\tau)]G(t_n-\tau,1)\,\mathrm{d}\tau\\&\quad\approx\left\{M(\tau_n)-h_1(\tau_n)\frac{\psi(t_n)+\psi(t_{n-1})}{2}\right\}\int_{t_{n-1}}^{t_n}G(t_n-\tau,1)\,\mathrm{d}\tau.\end{aligned} \tag{C.4}$$

Let us consider an auxiliary integral: $I(\bar{t})=\int_{t_{n-1}}^{\bar{t}}G(t_n-\tau,1)\,\mathrm{d}\tau$, where $\bar{t}\in(t_{n-1},t_n)$. In the range $[t_{n-1},\bar{t}]$ series (28) converges uniformly and absolutely as proven in Appendix B. Also, all terms of this series are continuous. Hence the order of summation and integration can be changed and using formula (28), we can write:

$$\begin{aligned}I(\bar{t})&=-2\kappa\sum_{m=1}^{\infty}\frac{\lambda_m^2}{h_0^2+h_0+\lambda_m^2}\int_{t_{n-1}}^{\bar{t}}\exp[-\kappa\lambda_m^2(t_n-\tau)]\mathrm{d}\tau\\&=-\sum_{m=1}^{\infty}\frac{2}{h_0^2+h_0+\lambda_m^2}\Big\{\exp[-\kappa\lambda_m^2(t_n-\bar{t})]\\&\quad-\exp[-\kappa\lambda_m^2\Delta t]\Big\}.\end{aligned} \tag{C.5}$$

The denominator in series (C.5) is always positive since $\|v_n\|^2>0$.

Remembering estimate (17), the series in (C.5) converges absolutely and uniformly for $\bar{t}\in[t_{n-1},t_n]$. Since all

terms in series (C.5) are continuous, the series is the continuous function as well. This allows us to consider the limit $\bar{t} \to t_n - 0$ in both parts of formula (C.5) to obtain

$$\begin{aligned}
&\int_{t_{n-1}}^{t_n} G(t_n - \tau, 1)\,\mathrm{d}\tau \\
&\quad = \lim_{\bar{t}\to t_n - 0} I(\bar{t}) \\
&\quad = -\sum_{m=1}^{\infty} \frac{2}{h_0^2 + h_0 + \lambda_m^2} \left\{ \lim_{\bar{t}\to t_n - 0} \exp[-\kappa\lambda_m^2 (t_n - \bar{t})] \right. \\
&\qquad \left. - \exp[-\kappa\lambda_m^2 \Delta t] \right\} \\
&\quad = -2\sum_{m=1}^{\infty} \frac{1}{h_0^2 + h_0 + \lambda_m^2} \left(1 - \exp[-\kappa\lambda_m^2 \Delta t]\right) \equiv g.
\end{aligned} \tag{C.6}$$

If $h_0 = 0$ then $\lambda_m = \pi(m - (1/2))$. The combination of formulae (C.3), (C.4) and (C.6) allows us to present Eq. (C.2) in the following form:

$$\begin{aligned}
\psi(t_n) = U(1, t_n) &- \{M(\tau_n) - h_1(\tau_n)[\psi(t_n) + \psi(t_{n-1})]/2\} g \\
&- \sum_{j=1}^{n-1} \{M(\tau_j) - h_1(\tau_j)[\psi(t_j) + \psi(t_{j-1})]/2\} \\
&\times G(t_n - \tau_j, 1)\Delta t,
\end{aligned} \tag{C.7}$$

where $n = 1, 2, \ldots, N$, and g is given by series (C.6).

Eq. (C.7) can be rearranged to the form particularly convenient for numerical analysis:

$$\begin{aligned}
\psi(t_n) = \frac{1}{1 - 0.5h_1(\tau_n)g} &\left\{ U(1, t_n) \right. \\
&- \left[M(\tau_n) - \frac{h_1(\tau_n)\psi(t_{n-1})}{2} \right] g \\
&- \sum_{j=1}^{n-1} \{M(\tau_j) - h_1(\tau_j)[\psi(t_j) + \psi(t_{j-1})]/2\} \\
&\left. \times G(t_n - \tau_j, 1)\Delta t \right\}.
\end{aligned} \tag{C.8}$$

For $n = 1$ the sum in formula (C.8) is equal to zero and $\psi(t_0)$ is a known constant (see above). This allows us to calculate $\psi(t_1)$ explicitly from formula (C.8). Once $\psi(t_1)$ has been calculated we can use formula (C.8) for calculation of $\psi(t_2)$ etc. At the nth step, formula (C.8) is used for calculation of $\psi(t_n)$ using the values of $\psi(t_0), \psi(t_1), \ldots \psi(t_{n-1})$ calculated at the previous steps. At this step all terms in the sum $\sum_{j=1}^{n-1}$ are already known. Once we have obtained the solution of Eq. (27) we can find the value of $u(r, \hat{t})$ from a discretised form of Eq. (23):

$$\begin{aligned}
u(r, \hat{t}) &= U(r, \hat{t}) - \sum_{j=1}^{N} \int_{t_{j-1}}^{t_j} \mu_{g0}(\tau) G(t - \tau, r)\,\mathrm{d}\tau \\
&= U(r, \hat{t}) - \sum_{j=1}^{N-1} \frac{\mu_{g0}(t_{j-1}) + \mu_{g0}(t_j)}{2} G(\hat{t} - \tau_j, r)\Delta t \\
&\quad - \frac{\mu_{g0}(t_{N-1}) + \mu_{g0}(t_N)}{2} \int_{t_{N-1}}^{t_N} G(t_N - \tau, r)\,\mathrm{d}\tau,
\end{aligned} \tag{C.9}$$

where $\hat{t} = t_N$. From estimate (25) it follows that the last integral is improper and needs to be calculated separately. Remembering Eq. (24), we can write

$$\begin{aligned}
&\int_{t_{N-1}}^{t_N} G(t_N - \tau, r)\,\mathrm{d}\tau \\
&\quad = -\kappa \sum_{n=1}^{\infty} \frac{\sin\lambda_n}{\|v_n\|^2} \sin\lambda_n r \int_{t_{N-1}}^{t_N} \exp[-\kappa\lambda_n^2 (t_N - \tau)]\mathrm{d}\tau \\
&\quad = -\sum_{n=1}^{\infty} \frac{\sin\lambda_n}{\|v_n\|^2} \frac{\sin(\lambda_n r)}{\lambda_n^2} [1 - \exp(-\kappa\lambda_n^2 \Delta t)] \\
&\quad = -2\sum_{n=1}^{\infty} \frac{h_0^2 + \lambda_n^2}{h_0^2 + h_0 + \lambda_n^2} \frac{\sin\lambda_n \sin(\lambda_n r)}{\lambda_n^2} [1 - \exp(-\kappa\lambda_n^2 \Delta t)].
\end{aligned} \tag{C.10}$$

When deriving this equation we took into account the expression for $\|v_n\|^2$ introduced in Eq. (A.9). This derivation is similar to the one given above (see Eq. (C.6)). Having substituted Eq. (C.9) into (C.8) we obtain the required value of $u(r, \hat{t})$. Note that $\mu_{g0}(t_j) = M(t_j) - h_1(t_j)u(1, t_j)$, where $u(1, t_j)$ is the solution of Eq. (C.8).

Appendix D. Investigation of the convergence of (29)

Let t_0 be an arbitrary fixed positive number and introduce the norm of the continuous function $F(t)$ for $t \in [0, t_0]$, $\|F\|_0 = \max_{0 \leqslant t \leqslant t_0} |F(t)|$. Let us rewrite the integral in the last equation in the system (31) as

$$v_j(t) = \int_0^t \eta(t - \tau) v_{j-1}(t - \tau) G(\tau, 1)\,\mathrm{d}\tau, \tag{D.1}$$

where $t \in [0, t_0]$. Hence, we can estimate the terms in series (29) as

$$\begin{aligned}
|v_j(t)| &\leqslant \int_0^t |\eta(t - \tau)||v_{j-1}(t - \tau)||G(\tau, 1)|\,\mathrm{d}\tau \\
&\leqslant \|\eta\|_0 \|v_{j-1}\|_0 \int_0^t |G(\tau, 1)|\,\mathrm{d}\tau \\
&\leqslant \|\eta\|_0 \|v_{j-1}\|_0 \int_0^t \frac{\tilde{c}}{\sqrt{\tau}}\,\mathrm{d}\tau \\
&= 2\tilde{c}\sqrt{t}\|\eta\|_0 \|v_{j-1}\|_0,
\end{aligned} \tag{D.2}$$

where $t \in [0, t_0]$. When deriving this estimate we took into account inequality (B.4) for $r = 1$.

Inequality (D.2) can be applied for v_{j-1}, v_{j-2} etc. This leads to the new estimate:

$$|v_j(t)| \leqslant (2\tilde{c}\sqrt{t}\|\eta\|_0)^2\|v_{j-2}\|_0 \leqslant \cdots \leqslant (2\tilde{c}\sqrt{t}\|\eta\|_0)^j\|v_0\|_0, \tag{D.3}$$

where v_0 is given by (31) and $t \in [0, t_0]$. Inequality (D.3) allows us to estimate series (29) as

$$\sum_{j=0}^{\infty}\epsilon^j|v_j(t)| \leqslant \sum_{j=0}^{\infty}\left(2\tilde{c}\epsilon\sqrt{t}\|\eta\|_0\right)^j\|v_0\|_0 \leqslant \sum_{j=0}^{\infty}\left(2\tilde{c}\epsilon\sqrt{t_0}\|\eta\|_0\right)^j\|v_0\|_0, \tag{D.4}$$

The series on the right-hand side of (D.4) is the geometrical progression which converges when $2\tilde{c}\epsilon\sqrt{t_0}\|\eta\|_0 < 1$, i.e. when

$$\epsilon\sqrt{t_0} < 1/\left(2\tilde{c}\|\eta\|_0\right), \tag{D.5}$$

where the constant $\tilde{c}$ is determined by (B.4). Based on the Weirschtrass criterion about uniform convergence of functional series, series (29) converges absolutely and uniformly for $t \in [0, t_0]$ if estimate (D.5) is valid. If t_0 is fixed then the criterion (D.5) can be rewritten as

$$\epsilon < 1/\left(2\tilde{c}\sqrt{t_0}\|\eta\|_0\right). \tag{D.6}$$

Note that series (29) converges not only for small ϵ but also for arbitrary fixed ϵ when t_0 is small enough. In this case criterion (D.6) needs to be replaced by the criterion: $t_0 < \left[1/\left(2\tilde{c}\epsilon\|\eta\|_0\right)\right]^2$. Let us now estimate the remainder of series (29) using inequality (D.3):

$$\left|\sum_{j=N+1}^{\infty}\epsilon^j v_j(t)\right| \leqslant \|v_0\|_0\sum_{j=N+1}^{\infty}\left(2\tilde{c}\epsilon\sqrt{t_0}\|\eta\|_0\right)^j = \|v_0\|_0\frac{\left(2\tilde{c}\epsilon\sqrt{t_0}\|\eta\|_0\right)^{N+1}}{1-2\tilde{c}\epsilon\sqrt{t_0}\|\eta\|_0} = \mathrm{O}\left((\epsilon\sqrt{t_0})^{N+1}\right). \tag{D.7}$$

Hence, it follows from series (29) that

$$v(t) = \sum_{j=0}^{N}\epsilon^j v_j(t) + \mathrm{O}\left((\epsilon\sqrt{t_0})^{N+1}\right), \tag{D.8}$$

where $t \in [0, t_0]$ and estimate (D.5) is assumed to be valid.

Appendix E. Approximations for $w(r)$

Results of experimental measurements of κ_λ for typical diesel fuels in the range 0.2–6 μm are shown in Fig. 6 (see [33] for the description of the experimental techniques used).

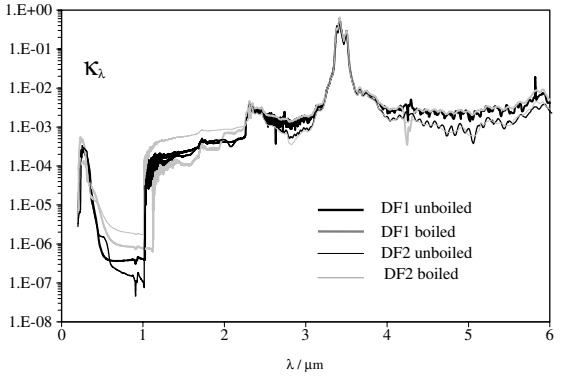

Fig. 6. Spectral distribution of the index of absorption κ_λ of low sulfur ESSO AF1313 diesel fuel used in cars (DF1: boiled and unboiled) and BP Ford reference diesel fuel used in off road equipment (DF2: boiled and unboiled).

The values of $w(r)$ were calculated based on the following equations [25]:

$$w(r) = \frac{[1-\mu_*\Theta(r-1/n)](r^2+\bar{\gamma})}{\left[0.6\left(1-\mu_c^5\right)-\mu_c^3/n^2\right]+\bar{\gamma}\left(1-\mu_c^3\right)}, \tag{E.1}$$

where

$$\bar{\gamma} = \frac{1.5}{\tau_0^2} - \frac{0.6}{n^2}, \quad \mu_* = \sqrt{1-\left(\frac{1}{nr}\right)^2},$$

$$\mu_c = \sqrt{1-\left(\frac{1}{n}\right)^2}, \quad \tau_0 = a_\lambda R_\mathrm{d} = 4\pi\kappa_\lambda R_\mathrm{d}/\lambda,$$

$$\Theta(x) = \begin{cases} 0 & \text{when } x < 0 \\ 1 & \text{when } x \geqslant 0 \end{cases}$$

and

$$w(r) = \frac{\xi^2\tau_0^3}{3}\frac{\exp\left[-\xi(\tau_0-\tau)\right]}{\tau_0(\xi\tau_0-2)+(2/\xi)[1-\exp(-\xi\tau_0),]}, \tag{E.2}$$

where $\tau = a_\lambda R$, $\xi = 2/(1+\mu_c)$. Eq. (E.1) was used when $\tau_0 < n\sqrt{2.5}$, otherwise Eq. (E.2) was used. The generalisation of the model presented in [23] to the case of asymmetrically illuminated droplet have been reported in [34].

References

[1] L.A. Dombrovsky, Thermal radiation from nonisothermal spherical particles of a semitransparent material, Int. J. Heat Mass Transfer 43 (2000) 1661–1672.

[2] L.A. Dombrovsky, S.S. Sazhin, E.M. Sazhina, G. Feng, M.R. Heikal, M.E.A. Bardsley, S.V. Mikhalovsky, Heating and evaporation of semi-transparent diesel fuel droplets in the presence of thermal radiation, Fuel 80 (2001) 1535–1544.

[3] W.A. Sirignano, Fluid Dynamics and Transport of Droplets and Sprays, Cambridge University Press, 1999.
[4] S.K. Aggarwal, A review of spray ignition phenomena: present status and future research, Prog. Energy Combust. Sci. 24 (1998) 565–600.
[5] S.S. Sazhin, G. Feng, M.R. Heikal, I. Goldfarb, V. Goldshtein, G. Kuzmenko, Thermal ignition analysis of a monodisperse spray with radiation, Combust. Flame 124 (2001) 684–701.
[6] E.M. Sazhina, S.S. Sazhin, M.R. Heikal, V.I. Babushok, R. Johns, A detailed modelling of the spray ignition process in Diesel engines, Combust. Sci. Tech. 160 (2000) 317–344.
[7] S.V. Utyuzhnikov, Numerical modeling of combustion of fuel-droplet-vapour releases in the atmosphere, Flow, Turbulence Combust. 68 (2002) 137–152.
[8] G.N. Gorelov, V.A. Sobolev, E.A. Schepakina, Singularly Perturbed Combustion Models, Samara State University Publishing House, 1999 (in Russian).
[9] L.A. Dombrovsky, L.I. Zaichik, Conditions of thermal explosion in a radiating gas with polydisperse liquid fuel, High Temperatures 39 (2001) 604–611.
[10] V. Bykov, I. Goldfarb, V. Gol'dshtein, J.B. Greenberg, Thermal explosion in a hot gas mixture with fuel droplets: a two reactant model, Comb. Theory Modell. 6 (2002) 339–359.
[11] C. Bertoli, M. Migliaccio, A finite conductivity model for diesel spray evaporation computations, Int. J. Heat Fluid Flow 20 (1999) 552–561.
[12] V.G. Levich, Physicochemical Hydrodynamics, Prentice-Hall, Englewood Cliffs, NJ, 1962.
[13] B. Abramzon, W.A. Sirignano, Droplet vaporization model for spray combustion calculations, Int. J. Heat Mass Transfer 32 (1989) 1605–1618.
[14] M.P. Mengüç, R. Viskanta, C.R. Ferguson, Multidimensional modelling of radiative heat transfer in Diesel engines, SAE Technical Paper 850503, 1985.
[15] P.F. Flynn, R.P. Durrett, G.L. Hunter, A.O. zur Loye, O.C. Akinyemi, J.E. Dec, C.K. Westbrook, Diesel combustion: an integrated view combining laser diagnostics, chemical kinetics, and empirical validation, SAE Report 1999-01-0509, 1999.
[16] R.Z. Kavtaradze, Local Heat Transfer in Reciprocating Engines, Moscow State Technical Bauman University Publishing House, 2001 (in Russian).
[17] L.A. Dombrovsky, S.S. Sazhin, A parabolic temperature profile model for heating of droplets, ASME J. Heat Transfer 125 (2003) 535–537.
[18] L.A. Dombrovsky, S.S. Sazhin, A simplified non-isothermal model for droplet heating and evaporation, Int. Commun. Heat Mass Transfer 30 (2003) 787–796.
[19] H.S. Carslaw, J.C. Jaeger, Conduction of Heat in Solids, Clarendon Press, Oxford, 1986.
[20] A.V. Luikov, Analytical Heat Transfer Theory, Academic Press, 1968.
[21] E.M. Kartashov, Analytical Methods in the Heat Transfer Theory in Solids, Vysshaya Shkola, Moscow, 2001 (in Russian).
[22] S.L. Bertoli, Radiant and convective heat transfer on pneumatic transport of particles: an analytical study, Int. J. Heat Mass Transfer 43 (2000) 2345–2363.
[23] L.A. Dombrovsky, S.S. Sazhin, Absorption of thermal radiation in a semi-transparent spherical droplet: a simplified model, Int. J. Heat Fluid Flow 24 (2003) 919–927.
[24] L.A. Dombrovsky, S.S. Sazhin, Absorption of thermal radiation inside a fuel droplet, in: P. Lybaert, V. Feldheim, D. Lemonnier, N. Selcuk (Eds.), Proc. Eurotherm Sem. Computational Thermal Radiation in Participating Media, Mons, Belgium, 15–17 April 2003, Elsevier, 2003, pp. 249–258.
[25] L.A. Dombrovsky, S.S. Sazhin, S.V. Mikhalovsky, R. Wood, M.R. Heikal, Spectral properties of diesel fuel droplets, Fuel 82 (2003) 15–22.
[26] J.S. Chin, A.H. Lefebvre, Steady-state evaporation characteristics of hydrocarbon fuel drops, AIAA J. 21 (1983) 1437–1443.
[27] A.H. Lefebvre, Atomization and Sprays, Taylor & Francis, 1989.
[28] A.P. Kryukov, V.Yu. Levashov, S.S. Sazhin, Evaporation of diesel fuel droplets: kinetic versus hydrodynamic models, Int. J. Heat Mass Transfer, in press.
[29] A. Crespo, A. Liñan, Unsteady effects in droplet evaporation and combustion, Combust. Sci. Technol. 11 (1975) 9–18.
[30] S.S. Sazhin, P.A. Krutitskii, A conduction model for transient heating of fuel droplets, in: H.G.W. Begehre, R.P. Gilbert, M.W. Wong (Eds.), Proc. 3d Intern. ISAAC (International Society for Analysis, Applications and Computations) Congress (August 20–25, 2001, Berlin), Progress in Analysis, vol. II, World Scientific, Singapore, 2003, pp. 1231–1239.
[31] G. Pitcher, G. Wigley, M. Saffman, Velocity and drop size measurements in fuel sprays in a direct injection Diesel engine, Particle and Particle Syst. Charact. 7 (1990) 160–168.
[32] M.A. Comer, P.J. Bowen, C.J. Bates, S.M. Sapsford, R.J.R. Johns, Transient 3D analysis of a DI gasoline engine injector spray, Atom. Sprays 9 (1999) 467–482, 1999.
[33] S.S. Sazhin, W.A. Abdelghaffar, E.M. Sazhina, S.V. Mikhalovsky, S.T. Meikle, C. Bai, Radiative heating of semi-transparent diesel fuel droplets. ASME J. Heat Transfer, in press.
[34] L.A. Dombrovsky, S.S. Sazhin, Absorption of external thermal radiation in asymmetrically illuminated droplets, J. Quantitative Spectrosc. Radiat. Transfer, in press.